j Med Imaging(ScholarGen) Volume 4(2021) 01, pp. 1-12 ISSN : 2635-4608

DOI http://dx.doi.org/10.31916/sjmi2021-01-01

1H MRS Analysis Using Ultrashort-TE Sequence of Hepatic Lipids in a 9.4T MRI Device

Jooyeon Kim

,Received : 25 June 2021 / Accepted : 22 November 2021 / Published online 28 December 2021

Abstract Non-alcoholic fatty liver disease is the most common cause of chronic liver diseases which is characterized by the increased level in obesity, and diabetes. Liver lipid content has been suggested to play an important pathogenic role in the development of liver fibrosis, and cirrhosis In particular, it is associated with the risk of hepatocellular carcinoma (HCC). Liver biopsy is still the gold standard for diagnosing and assessing the disease. However, the invasive and limited tissue sampling of the biopsy presents problems. Proton magnetic resonance spectroscopy (^{1}H-MRS) enables the study of cellular biochemistry and metabolism and provides a non-invasive means to determine disease abnormalities and progression in vivo and longitudinally. With the increased availability of high-field magnetic resonance (MR) systems for clinical and preclinical studies, both signal-to-noise ratio (SNR) and spectral resolution of metabolites in the MR spectra can be improved significantly, allowing more accurate metabolite identification, quantification and thus disease characterization. ^{1}H-MRS permits longitudinal assessment of fat fraction, saturated and unsaturated. This study is to characterize early hepatic lipid changes in fatty liver mouse model by in vivo short-echo time (TE) ^{1}H-MRS (Proton-Magnetic Resonance Spectroscopy).

This study examined 17 male C57BL/6 mice, including 8 high-fat diet (45%) mice for 20 weeks and 9 normal mice for 17 weeks. C57BL/6 mices were fed with 60% high fat diet containing 60% fat, 20% protein and 20% carbohydrate. MR imaging with single-voxel ^{1}H-MRS was performed using a PRESS sequence at 9.4T magnetic resonance imaging (MRI). The full width at half maxium (FWHM) ranged from 4 to 8 Hz. Water suppression was accomplished with "VAPOR" pulses. The examination (voxel size, 2×2×2 mm^3) were performed from liver parenchyma in mice at normal and at high-fat diet, respectively. The spectral acquisition parameters were TR/TE = 2500/16 ms, and 256 acquisitions for averaging. LCModel fitting was conducted using experimental basis sets. Less than 10% standard deviation (%SD) of metabolite quantification data was allowed. The areas under the peaks were measured as the follows: signal integrals of lipid methyl protons (-CH_3; 0.9 ppm), methylene proton ((-CH_2-)n; 1.3 ppm), allylic protons (-CH_2-C=C-CH_2, 2.1 ppm), α-methylene protons (-CO-CH_2-CH $_2$; 2.3 ppm), diallylic protons (=CCH-$_2$C=; 2.8 ppm), glycerol protons (CH_2-COO; 4.1 ppm), glycerol protons (CH_2-COO; 4.3 ppm) and methene protons (CH=CH; 5.3 ppm). For relative quantification, total lipid (TL), total saturated fatty acid (TSFA), total unsaturated fatty acid (TUFA), total unsaturated bond (TUB), polyunsaturated bond (PB) and choline-containing compound (Cho) were normalized by separating each peak of (-CH2-)n, -CH_2-C=C-CH_2-, -CO-CH_2-CH_2=C-CH-$_2$-C= and –CH=CH-.

[1]***Jooyeon Kim***(✉)
Department of Research Equipment Operation
Korea Basic Science Institute, Cheong-won, Ochang,
Republic of Korea

Significant increases in lipid signals of 0.9, 1.3, 2.1, 2.3, 2.8, 4.1, 4.3, and 5.3 ppm were found in animals at high-fat diet($p<0.01$, $p<0.001$). TL, TSFA, TUFA, TUB, PUB and Cho were significantly increased at high-fat diet($p<0.01$, $p<0.05$). Therefore, ^{1}H-MRS is useful in detecting and characterizing various hepatic lipid alterations.

Key word : Fat liver; Hepatic lipids; MRS; Ultrashort TE; 9.4T MRI

1. INTRODUCTION

Obesity increases death rate by causing liver disease, diabetes, gallstones, chronic hepatitis, cerebrovascular disorders, and heart disease[1]. There is NAFLD(non-alcoholic fatty liver disease) in liver disease that causes obesity. NAFLD is a disease in which triglycerides are accumulated in hepatocytes regardless of alcohol consumption. Currently, 30% of the total population falls under NAFLD, and 90% of patients who underwent surgery for severe obesity are considered to be due to NAFLD[2]. NAFLD is associated with obesity and diabetes, and liver lipid content has been known to play an important role in the development of liver fibrosis and cirrhosis[3]. Animal model experiments for hepatocellular carcinoma are starting, but additional studies are needed for treatment, diagnosis, and prevention[4].

1H-MRS can provide the chemical structure or state of metabolites in vivo in a non-invasive method[5], and has been used to diagnose non-alcoholic fatty liver disease[6]. Recently, the development of high magnetic field devices has greatly improved the signal-to-noise ratio (SNR) and resolution of magnetic resonance imaging system.

Therefore, it is necessary to identify and quantify metabolites in vivo using a high magnetic field magnetic resonance system to determine the characteristics of NAFLD[7]. The high magnetic field magnetic resonance imaging system can analyze the signals of lipid metabolites such as total lipid, total saturated fatty acid, total unsaturated fatty acid, total unsaturated bond, and polyunsaturated bond using 1H-MRS. Choline-containing compounds can be analyzed using 1H-MRS through signal integration of Lipid methyl protons(-CH_3; 0.9 ppm), Methylene protons((-CH_2-)n; 1.3 ppm), Allylic protons(-CH_2-C=C-CH_2; 2.1 ppm), α-methylene protons(-CO-CH_2-CH_2; 2.3 ppm), Diallyic protons(=C-CH_2-C=; 2.8 ppm), and methene protons(-CH=CH-; 5.3 ppm) (Cheung et al. 2011).

The purpose of this study was to analyze liver lipid metabolites and fatty acid components of normal mouse and fatty liver mouse through 1H-MRS using ultra-high magnetic field 9.4T MRI. We are trying to characterize non-alcoholic fatty liver disease through analysis.

2. EXPERIMENTAL METHODS

2.1. Experimental animals

The experiment was conducted for 20 weeks. In the laboratory environment, the temperature was set to 22 degrees Celsius, and the humidity was set to 50% to 60% and checked every 12 hours. A total of 17 animals were divided into 8 control animals and 9 experimental groups. The control group was fed a general diet containing mainly carbohydrates and proteins, and the experimental group was fed a high-fat diet containing 60% carbohydrates, 20% fat, and 20% protein. The weight and blood glucose levels of the control and experimental mice were measured for each week of age. Breathing was monitored, and warm water was circulated through the heating pad to maintain body temperature at 36.5 degrees.

Pulse sequence for MRI used a PRESS(point-resolved spectroscopy) sequence. After the MRI experiment, for histopathological evaluation, liver tissue was excised and the liver samples were fixed

in formalin. The sufficiently fixed tissue was washed with water to remove an excessive amount of fixing reagent. In order to embedding by infiltrating paraffin that does not mix with water into the liver tissue, the liver tissue was dehydrated using alcohol with a difference in concentration. Dehydration was gradually processed from a low-concentration alcohol solution to a high-concentration alcohol solution, followed by treatment with pure 100% alcohol and benzene. Paraffin dissolved in benzene as an organic solvent was penetrated into the dehydrated tissue, and then treated with pure paraffin in the liquid state at high temperature (60°C) to completely penetrate. The paraffin that has penetrated into the tissue was cooled at low temperature to make a solid-state, and then cut into appropriate size and trimmed. It was cut to an appropriate thickness(3~20 μm) in a thin-cutting machine. The sliced tissue adhered to a glass slide, and tissue paraffin was removed with xylene, an organic solvent. Since most staining solutions are aqueous solutions, the slides with liver tissues were hydrated by treating them with a high concentration of alcohol to a low concentration of alcohol aqueous solution. Primary staining was performed with an aqueous hematoxylin solution. At first, after staining it thick, it was stained through the process of properly matching the staining degree of the sample that was excessively stained with an alcohol solution. Then, secondary staining was performed with eosin. Hematoxylin was stained blue when it encountered acids such as the nucleus of cells and other acidic structures (the cytoplasm is rich in RNA, cartilage matrix). And eosin met basicity and stained other cytoplasmic components and collagen in red. After the first and second staining was done, a microscopic examination was performed. The stained results were read by two pathologists. The level was decided by comparing the liver of the control group and the liver of the experimental group with the level of the pathology score. As a result of the comparison, the degree of fat content and the degree of inflammation were discriminated from 0 to 3.

2.2. 9.4T MRI

A number of studies have been performed on the imaging of mice using 9.4T MRI equipment[8]. The purpose of this study is to find a method for diagnosing non-alcoholic fatty liver similar to an invasive histopathological examination by confirming that the signals of lipid metabolites are clearly different in 9.4T MRI for animals. This is because the recent introduction of the high magnetic field (≥3.0 Tesla) MRI devices is expanding, and high magnetic field MRI devices provide high SNR and spectrum resolution so that the peaks for each material are well separated in MRS. The 4-channel animal coil used in this experiment is a 9.4T-only coil, and it is able to greatly improve SNR and resolution by putting it closer to the experimental mouse. Figure 1(a) is a 9.4 Tesla (Broker System 9.4T animal MRI device) and Figure 1(b) is a picture of a 4-channel mouse heart receive-only animal coil.

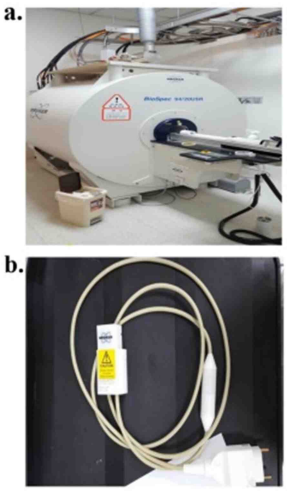

Figure 1. Broker system 9.4T animal MRI(a) and a 4-channel mouse heart receive-only array animal coil(b)

2.3. MR signal acquisition

In 9.4 T MRI, T2-weighted fast spin-echo was used to obtain the transverse, sagittal, and coronal (FOV 60 mm × 60 mm, slice thickness = 1.5 mm) in the axial direction of three sections. 1H-MRS used a Point-resolved spectroscopy (PRESS) sequence[9]. In order to determine the 3D position of the ROI with the PRESS sequence, a 90° slice selective RF pulse and a 180° RF pulse are applied twice[10]. During the 90° pulse stimulation, the z-direction slice is determined by the gradient magnetic field GZ. During the following two 180° pulse stimuli, Gy and Gx determine the thickness of the slices in the y and x directions, similar to the principle of determining the z-direction slice, and the volume of interest is determined as the intersection point of the three slices found.

As a parameter, TR/TE = 2500/16 ms was used, and data were obtained with a matrix size of 256. The single voxel method was used, and the voxel size was 2×2×2 mm^3 so that the largest blood vessels were avoided and placed in the uniform liver parenchyma. In particular, the 1H-MRS voxel size can create a smaller voxel size as the magnetic field strength of the magnet increases, and in general, the optimal voxel amount is determined through the signal-to-noise ratio and scan time.

Typical water peak signals were suppressed using variable power and optimized relaxation delays (VAPOR) pulses, and the line width (FWHM) included 37-69 Hz (mean±SD, 52.1±9.62 Hz). For each lipid metabolite, the baseline was 0 weeks before feeding the high-fat diet, and the concentration values of the metabolites were measured and the percent (%) was calculated by comparing by week age.

Lipid metabolites below the peak are listed in Table 1, Lipid methyl protons (-CH3; 0.9 ppm), Methylene protons ((-CH2-)n; 1.3 ppm), and Allylic protons (-CH2-C=C-CH2; 2.1 ppm).), α-methylene protons (-CO-CH2-CH2; 2.3 ppm), Diallylic protons (=C-CH-2-C=; 2.8 ppm), glycerol protons (CH2-COO; 4.1 ppm), glycerol protons (CH2 -COO; 4.3 ppm) and methene protons (-CH=CH-; 5.3 ppm) were measured [11]. Fatty acid components of each of these lipid metabolites were calculated using a mathematical formula, and the percentage (%) was obtained by measuring the concentration of the metabolite by comparing each week with age 0 weeks before feeding the high-fat diet.

Fatty acid components in Table 2 are total lipid, total saturated fatty acid, total unsaturated fatty acid, total unsaturated bond, polyunsaturated bond, It was measured as choline (Choline-containing compound, CCC)[12]. Considering the fact that the SNR is similar between spectra due to the same voxel size and hardware configuration for total lipid and choline, (-CH2-)n, CCC was quantified by dividing the peak by spectral noise. In addition, total saturated fatty acid, total unsaturated fatty acid, total unsaturated mixture, polyunsaturated mixture were peaked by (-CH2-)n, -CH2-C=C-CH2, -CH=CH-, =C-CH-2-C by –CH3 Was quantified by dividing[13].

Table 1. Peak area ratio of various metabolite name in proton magnetic name in proton magnetic resonance spectroscopy(^{1}H-MRS)

No	Name	Peak area ratio	Chemical shift
1	methyl	$-CH_3$	0.9 ppm
2	methylene	$-(CH_2)_n-$	1.3 ppm
3	allylic	$-CH_2-CH=CH-CH_2-$	2.1 ppm
4	α-methylene	$-CO-CH_2-CH_2$	2.3 ppm
5	diallylic	$-CH=CH-CH_2-CH=CH-$	2.8 ppm
6	glycerol	CH_2-COO	4.1 ppm
7	glycerol	CH_2-COO	4.3 ppm
8	vinyl	-CH=CH-	5.3 ppm

Table 2. Fatty acid ratios and resonant frequency(ppm) in proton magnetic resonance spectroscopy(^{1}H-MRS)

Index of fatty acid	Fatty acid component
Total lipid	Lip13
Total saturated fatty acid	3×Lip13/2×Lip09
Total unsaturated fatty acid	3×Lip20/4×Lip09
Total unsaturated bond	3×Lip53/2×Lip09
Polyunsaturated bond	3×Lip28/2×Lip09
Choline-containing compound (CCC)	Lip32

2.4 Sattistical analysis

Raw data obtained through 1H-MRS were analyzed using LCModel software (Linear Combination of Model, Version 6.3-1H, Stephen W. Provencher). LCModel is a widely used algorithm, and it is a method of quantifying magnetic resonance spectroscopy using a semi-parametric NLLS(Non Linear Least Square) method based on a priori information through metabolite base set. The model is built on the basis of the real part of the Fourier transformed spectrum and consists of two parts. The first is the term that describes the baseline, and the second is the term that describes the spectral line shape.

The model is as follows.

$$\hat{Y}[\nu_k] = e^{-i(\phi_0+\nu_k\phi_1)}\left[\sum_{j=1}^{N_B}\beta_j B_j(\nu_k)+\sum_{l=1}^{N_M}c_l\sum_{n=-N_S}^{N_S}S_n M_l(\nu_{k-n};\gamma_l,\epsilon_l)\right]$$

$$Y[\nu_k] = \hat{Y}[\nu_k] + \epsilon[\nu_k] \quad \text{---------- (1)}$$

What we want to find in the end using the model is to find P, B, and S that satisfy the conditions that minimize the equation below.

$$\frac{1}{\sigma^2(Y)}\sum_{k=1}^{N}(R[Y(\nu_k)-\hat{Y}(\nu_k)])^2+\|\alpha_C R_C S\|^2+\|\alpha_B R_B B\|^2+\sum_{l=1}^{M}\left(\frac{|\gamma_l-\gamma_l^0|^2}{\sigma^2(Y)}+\frac{\epsilon_l^2}{\sigma^2(\epsilon_l)}\right)$$

Constraint : $\gamma_1 \geq 0, \epsilon_l \geq 0, \sum S = 1$ ---------- (2)

This minimization process is performed using CONTIN, a uniform nonlinear least-squares method developed by Dr. Provencher[14]. The baseline of the spectrum is modeled by LCModel using the cubic B-spline method. In addition, the metabolite database obtained by in vitro measurement or simulation is stored internally in the LCModel[15]. The error estimation is given through the CRLB(Cramer-Rao lower bound), where CRLB is the theoretical minimum of the variance (σ2) that an estimator (e.g., metabolite concentration) can take. And is defined as the inverse of Fisher's information F as follows.

$$\sigma^2 \geq F^{-1} = CRLB$$

$$F = E\left[\left(\frac{\partial \ln L}{\partial p}\right)^T\left(\frac{\partial \ln L}{\partial p}\right)\right] \quad \text{---------- (3)}$$

Here, L represents a likelihood function, p=(P1,P2,...,PN) represents a model parameter, T represents a transpose, and E represents an expectation value. In general, a likelihood function is assumed to determine what distribution the rest, which is the difference between the measured data and the model function, will be shown. In the case of LCModel, it has not yet been reported how to accurately calculate CRLB[16]. This algorithm requires a base set, a collection of pure metabolite spectra, in order to quantify the concentration of metabolites present in the acquired signal. The metabolite signals that make up the base set are fitted to the acquired spectrum, which includes a spline function to model the lower part of the spectrum baseline due to a sufficiently uninhibited water signal or macromolecules. For linear combination model fitting, an experimental basis set (LCModel provoded) was used. For the basis set, curve fitting was performed using the basis set

provided by LCModel. A standard deviation (%SD) of less than 10% of the lipid metabolite quantification data was allowed. Error estimation was used as a useful reliability indicator through the CRLB named %SD. In order to see the difference in fatty acids quantified in the liver of normal mouse and in the liver of mouse induced by a high fat diet, SPSS version 21 software package (SPSS, Chicago, IL, USA) was used to analyze. For each interlipid metabolite and fatty acid component, it was expressed as mean ± standard deviation. Paired student's t-test was performed. At this time, a value of $p<0.05$ was judged to have statistical significance.

3. RESULT

For the experiment, 6-week-old male mice (C57BL/6 mice) weighting 20±5 gram were fed a general diet to 8 control animals, and 9 mice in the experimental group were fed a high fat diet(fat-60%, protein-20%, Carbohydrates -20%) were fed. Thereafter, at 20 weeks, the parenchymal tissues of 9 mice in the experimental group were examined.

3.1. Fatty liver mouse model weight and blood glucose level comparison by week

Figure 2(a) shows the results of measuring the weight of the control group and the experimental group for each week. After 6 weeks, the control group was 26.4±3.24 g and the experimental group was 28.8±2.20 g. These results indicate statistical significance ($p<0.05$) (Table 3). In addition, Figure 2(b) shows the blood glucose measurement results after 11 weeks. As a result of measuring blood glucose, the control group was 98.7±2.34 g and the experimental group was 136±3.20 g. This result also showed a statistically significant increase ($p<0.01$) (Table 4).

Table 3. Body weight(g) indices in proton magnetic resonance spectroscopy (^{1}H-MRS) at 9.4T MRI

Week	Normal	High-fat diet	*P*-value
0	20.5	20.5	0.000
3	24.4	25.7	0.116
6	26.4	28.8	0.019
7	26.7	31.4	0.001
8	26.9	31.9	0.001
9	27.6	32.8	0.000
10	28	34.2	0.000
11	29	35.2	0.002
12	28.2	35.5	0.000
13	27.7	35.1	0.000
14	28.2	37.2	0.000
15	28.7	38.5	0.000
16	28.6	39.3	0.000
17	28.6	39.9	0.000
18	28.9	40.2	0.000

Table 4 Blood sugar indies in proton MRS at 9.4 T MRI

Week	Normal	High-fat diet	*P*-value
8	102.6	110.8	0.210
11	97.6	127.6	0.002
13	147.6	169.3	0.001
16	139.3	170.8	0.008
17	138	170.8	0.009

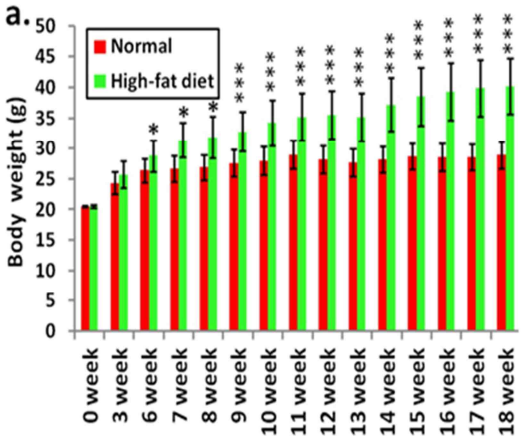

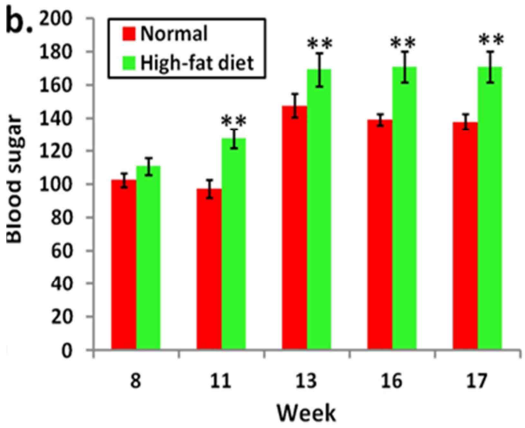

Figure 2. Body weight(g)(a) and blood sugar(b) in normal mice compared to high fat mice. Data shows mean±SD for each group using a two tailed *t*-test with significance threshold of *p<0.05, **p<0.01, ***p<0.001.

3.2. Comparison of liver lipid metabolites in vivo

Through 1H-MRS, the metabolites of interlipid metabolites corresponding to 0.9, 1.3, 2.1, 2.3, 2.8, 4.1, 4.3 and 5.3 ppm are shown. Through this, it can be seen that the corresponding interlipid metabolites appear differently for each frequency. Interlipid metabolites corresponding to 4.1 and 4.3 ppm, which were not seen in previous 3T MRI, were found. Lipid metabolites below the peak were measured as shown in Table 7. Figure 3 shows the comparison of the liver lipid metabolites of the control group and the liver lipid metabolites of the experimental group in 1H-MRS, and there was a statistically significant difference with an increase of 0.9 ppm (p<0.01). In addition, there was a statistically significant difference as 1.3, 2.3, 2.8, 4.1, 4.3 and 5.3 ppm increased (p<0.001) (Table 5).

Table 5. Lipid signals indies in proton magnetic resonance spectroscopy(^{1}H-MRS) at 9.4T MRI

Name	Normal	High-fat diet	*P*-value
Lip09	0.010	0.080	0.007
Lip13	0.066	0.466	0.000
Lip21	0.012	0.078	0.000
Lip23	0.006	0.060	0.000
Lip28	0.005	0.032	0.000
Lip41	0.005	0.023	0.000
Lip43	0.005	0.023	0.000
Lip53	0.011	0.106	0.000

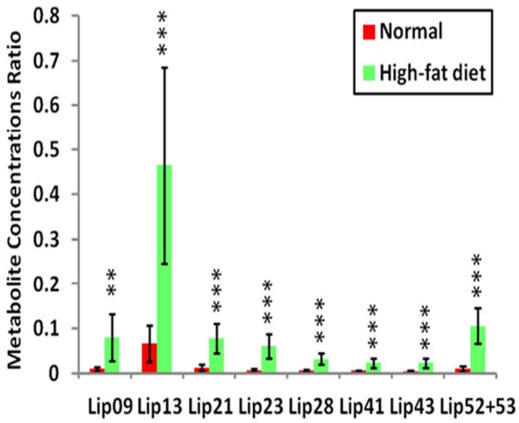

Figure 3. Lipid signals quantified normal and 20 weeks after high fat diet. Data shows mean±SD for each group using a two tailed *t*-test with significance threshold of **p<0.01, ***p<0.001.

3.3. Comparison of liver fatty acid components in vivo

Figure 4 shows the lipid metabolites obtained using a mathematical formula. The percentage (%) was calculated by comparing the liver fatty acid component of the control group and the liver fatty acid component of the experimental group. When comparing the liver fatty acid components of the control group and the liver fatty acid components of the experimental group, there was a statistically

significant difference due to an increase in total lipids ($p<0.01$). Also, there was a statistically significant difference due to the increase in saturated fatty acid, unsaturated fatty acid, unsaturated mixture, polyunsaturated mixture, and choline ($p<0.05$) (Table 6).

Table 6. Fat fraction indices in proton magnetic resonance spectroscopy(^{1}H-MRS) at 9.4T MRI

Name	Normal	High-fat	*P*-value
TL	0.066	0.466	0.001
TSFA	0.012	0.068	0.020
TUFA	0.010	0.054	0.038
TUB	0.018	0.087	0.011
PB	0.010	0.045	0.040
CCC	0.019	0.057	0.034
UI	0.108	0.155	0.030

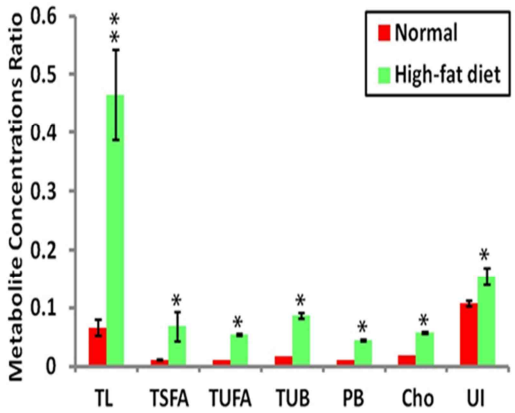

Figure 4. Fat fractions quantified normal and 20 weeks after high fat diet. Data shows mean±SD for each group using a two tailed *t*-test with significance threshold of *p<0.05, **p<0.01.

3.4. Histopathological evaluation

Figure 16(a) shows the comparison of hepatocytes of the control group and the hepatocytes of the experimental group. It was found that fat accumulation was significantly increased in the hepatocytes of the experimental group, and conventional cell necrosis and apoptosis were observed. Iron pigmentation is indicated in bright blue, nuclei in red, and cytoplasm in bright pink. Figure 16(b) shows that two pathologists compared the control liver cells and the experimental group liver cells with the mean pathology score level. As a result of comparison, the score of inflammation increased, but there was no statistically significant difference. On the other hand, the score of steatosis increased and was statistically significantly higher ($p<0.05$, $p<0.001$) (Table 13).

Table 7. Pathological score reading's indices of normal and high-fat diet liver in Hematoxylin-eosin (H&E) staining at Microscope

Reader	Name	Normal	High-fat	*P*-value
Reading 1	Inflammation	0.111	0.375	0.389
	Steatosis	0.222	2.250	0.000
Reading 2	Inflammation	0.111	0.375	0.378
	Steatosis	0.444	1.625	0.048

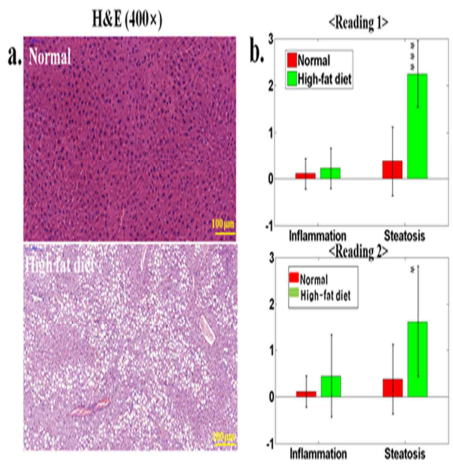

Figure 5. Typical hematoxylin-eosin(H&E) staining(400×; left column) normal liver(a, top) and livers subjected to high-fat diet liver(a,bottom) and pathological scores for 20 weeks(b). Data shows mean±SD for each group using a two tailed *t*-test

with significance threshold of *p<0.05, ***p<0.001.

4. Discusion

In this study, it was demonstrated that 1H-MRS can be used to detect interlipid abnormalities in fatty liver disease. The 1H-MRS is the most standard MR image scanner for obtaining high-resolution images and functional information. It has been used to investigate local liver lesions and has been found to be useful by characterizing human and animal liver cancer models.

4.1. Difference between 1H-MRS PRESS and STEAM

Unlike ultrasonography, which subjectively determines the presence of fatty liver, 1H-MRS can non-invasively measure the visceral fat area and the degree of liver fat infiltration by objective values. Therefore, it is possible to diagnose fatty liver by accurately and quantitatively measuring it, and it is useful for follow-up observation of improvement in health status after diagnosis[17]. In this study, the highest magnetic field was used to study fatty liver compared to previous studies. At high magnetic fields, 1H-MRS provides a high-quality spectrum within an acceptable scan time due to the inclusion of a good SNR and increased spectral resolution. This study confirmed in vivo accurate biochemical information that can be used for characterization and monitoring of liver diseases including fatty liver in 9.4T MRI. In previous studies, it was relatively difficult to accurately analyze and quantify multiple lipid signals due to limited spectral resolution. On the other hand, in this study using 9.4T MRI, various lipid peaks (eg, -CH2-C=C-CH2-, =C-CH2-C=, -CH=CH-) were analyzed in the fatty liver. Through this, accurate information on the lipid composition was obtained. Currently, 1H-MRS is divided into two methods: a single voxel technique and a multi-voxel technique. The single-voxel technique is a single volume method that selects one 3D pixel at a local area in an MR image, and because this method can be obtained with a high-frequency resolution, it is easy to distinguish each metabolite and the data analysis time is short. The multi-voxel technique is a multi-volume method for obtaining multiple 3D pixels by adding an additional selective gradient. In this method, a CSI(chemical shift imaging) image is also possible to image information of specific metabolites from each location. STEAM(stimulated echo acquisition method) is a method of continuously giving three-time slice-selective 90° RF pulses. If three RF waves were selected on a right-angled plane, a stimulated echo would be obtained only in the volume of the three samples at the intersection of the right-angled planes. Generally, the CHESS pulse is used to suppress the water signal, and the size of the signal appears smaller than PRESS. In PRESS(point resolved spectroscopy), a 90° slice selective RF pulse is applied and then 180° RF pulses are applied twice. PRESS sequence is the same as the STEAM sequence and includes CHESS pulse waveform. If a 180° pulse is used and the SNR is approximately two times higher than that of stimulated echo by spin echo, it can be used in a local area of about 1 cc ($1\times1\times1$ cm^3). In the abdominal magnetic resonance spectroscopy test, because the SNR is low due to respiration, the PRESS method, which has an SNR of about 40% or more compared to the STEAM method, had superior results in this experiment.

4.2. Efficacy of high magnetic field 9.4T MRI

The characteristics of this study using high magnetic field 9.4T MRI are as follows.

(1) High magnetic field 1H-MRS can obtain information on various lipid metabolites by separating two peaks of lipid metabolites well. Through 9.4T MRI, the 4.1 and 4.3 peaks were well separated and information on various lipid metabolites could be obtained due to the high magnetic field's 1H-MRS resolution[18].

(2) Respiration was continuously monitored to reduce artifacts caused by respiration, and uniform hepatic parenchymal tissue was obtained using a long TR.

(3) In order to correct the non-uniform magnetic field to a uniform magnetic field, the noise was blocked in the region of interest by repeatedly shimming.

(4) The accuracy of quantification of fatty acid components was improved by examining pathological tissue specimens[19] .

4.3. Comparison of liver lipid metabolites and fatty acid components in vivo

When comparing lipids and saturated fatty acids 2 weeks after starting the high-fat diet, the concentration of metabolites was significantly increased ($p<0.01$). The most significant changes in lipid and saturated fatty acid showed that the increase of saturated fatty acid was mainly involved in the increase of lipid. It was found that the increase in lipid was due to fat infiltration and changes in hepatocytes. It was found that the increase of saturated fatty acid in the liver is related to activated cell death induced by saturated fatty acid[20]. In non-alcoholic fatty liver disease, endoplasmic reticulum stress associated with increased saturated fatty acids in the liver has been shown to promote liver damage. It partially contributed to the progression of diseases ranging from simple fatty liver to fatty hepatitis. In unsaturated fatty acids, unsaturated mixtures, and polyunsaturated mixtures, a significant increase in metabolite concentration was observed ($p<0.05$). More unsaturated double bonds were formed and increased in monounsaturated fatty acids 2 weeks after eating a high-fat diet[21]. This increased degree of polysaturation and increased cell necrosis and death were observed in various experimental models. After hematoxyline-eosin staining for histological evaluation, hepatic fat accumulation was confirmed [21]. In 2014, Pacifico and Scorletti, a study found that administration of n-3 PUFA affected non-alcoholic fatty liver. Therefore, the long-term administration of a high-fat diet may indirectly be a factor that may adversely affect the liver.

4.4. Limitation of this study and future studies

The limitations of this study are as follows. In 9.4T MRI, the age and number of mice in the control group and the experimental group are different. The experiment was attempted to be divided by week age as much as possible, but due to movement artifacts caused by breathing during the experiment, breathing monitoring had to be continuously performed, and it took a long time to perform one test, so the age of the week was different. There was a case where the experimental mice died during the experiment, and the number of the control group and the experimental group became insufficient. Therefore, in future studies, it is necessary to diversify the types of control and experimental groups, increase the number of experimental mice, and conduct experiments under the same conditions. If so, it is thought that it will be able to provide a new direction for accurate quantitative evaluation of liver disease models.

5. Conclusion

In this study, a hepatic steatosis model was established by verifying that the lipid signal in the liver parenchyma of mice increased for a long time

20 weeks after feeding a high-fat diet through 1H-MRS in a 9.4T MRI experiment. As a result of the evaluation by the histopathological method, it was not possible to confirm even a liver fibrosis model. In the future, by injecting a CCl4 solution into olive oil, various chemical substances secreted from kupffer cells, which are macrophages in the liver, change the phenotype of hepatocytes and astrocytes, thereby will test the mechanism of accumulation of extracellular matrix such as collagen. Based on this, we will establish a liver fibrosis model by magnetic resonance spectroscopy. In addition, the high magnetic field 1H-MRS and MRI will be useful for diagnosing fatty liver by accurately measuring the visceral fat area and liver fat infiltration degree non-invasively, and for follow-up observation of improvement in health status after diagnosis. If such research is carried out continuously, it will be possible to develop new therapeutic drugs and propose new treatment methods by analyzing changes in a wide range of metabolites through quantitative evaluation of liver disease models.

[Reference]

[1] Fabbrini, E., Sullivan, S. and Samuel, K. (2010). "Obesity and nonalcoholic fatty liver disease: biochemical, metabolic, and clinical implications," *Hepatology,* 51(2), 679-689.

[2] Angulo, P.(2002), "Nonalcoholic fatty liver disease," *New England Journal of Medicine,* 346(16), 1221-1231.

[3] Ekstedt, M., Franzen, L. E., Mathiesen, U. L., Mathiesen, L., Thorelius, L., Holmqvist, M. and Bondemar, G.(2006). "Long-term follow-up of patients with NAFLD and elevated liver enzymes," *Hepatology,* 44(4), 865-873.

[4] Bataller, R. and Brenner, D. A.(2005), "Liver fibrosis," *The Journal of clinical investigation,* 115(2), 209-218.

[5] Zhong, K. and Emst, T.(2004), "Localized in vivo human 1H MRS at very short echo times," *Magnetic Resonance in Medicine: An Official Journal of the International Society for Magnetic Resonance in Medicine,* 52(4), 898-901.

[6] Marsman, H. A., Van Werven, J. R., Nederveen, A. J., Ten Kate, F. J. Heger, M., Stoker, J. and Van Gulik, T. M.(2010), "Noninvasive Quantification of Hepatic Steatosis in Rats Using 3.0 T ^{1}H-Magnetic Resonance Spectrosopy," *Journal of Magnetic Resonance Imaging*, 32(1), 148-154.

[7] Hamilton, G., Middleton, M. S., Bydder, M., Yokoo, T., Schwimmer, J. B., Kono, Y., Patton, H. M., Lavine, J. E. and Sirlin, C. B.(2009), "Effect of PRESS and STEAM sequences on magnetic resonance spectroscopic liver fat quantification," *Journal of Magnetic Resonance Imaging: An Official Journal of the International Society for Magnetic Resonance in Medicine,* 30(1), 145-152.

[8] Lee, Y. J., Jee, H. J., Noh, H. J., Kang, G. H., Park, J. Y., Cho, J. G., Cho, J. H., Ahn, S. D., Lee, C. H., Kim, O. H., Oh, B. C. and Kim, H. J.(2013), "In Vivo ^{1}H-MRS Hepatic Lipid Profiling in Nonalcoholic Fatty Liver Disease: An Animal Study at 9.4T," *Magnetic resonance in medicine,* 70(3), 620-629.

[9] Bazelaire, D., Cedric, M. J., Duhamel, G. D., Rofsky, N. M. and Alsop. D. C.(2004), "MR imaging relaxation times of abdominal and pelvic tissues measured in vivo at 3.0 T," *Hepatology,* 230(3), 652-659.

[10] Bottomley. and Paul, A.(1987), "Spatial localization in NMR spectroscopy in vivo," *Annals of the New York Academy of Sciences,* 508(1), 333-348.

[11] Lim, A. K., Hamilton, G., Patel, N., Jimmy, J. D. and Taylor-Robinson, S. D.(2013), "1H MR spectroscopy in the evaluation of

the severity of chronic liver disease," *Radiology,* 226(1), 288-289.

[12] Johnson, J. A., Walton, D. W., Sachinwalla, T., Thompson, C. H., Smith, K., Ruell, P. A., Stannard, S. R. and George, J.(2008), "Noninvasive Assessment of Hepatic Lipid Composition: Advancing Understanding and Management of Fatty Liver Disorders," *Hepatology,* 47(5), 757-763.

[13] Corbin, I. R., Furth, E. E., Pickup, S., Siegelman, E. S., and Delikatny, E. J.(2009), "In vivo assessment of hepatic triglycerides in murine non-alcoholic fatty liver disease using magnetic resonance spectroscopy," *Biochimica et Biophysica Acta (BBA)-Molecular and Cell Biology of Lipids,* 1791(8), 757-763.

[14] Provencher, S. W.(1982). "A constrained regularization method for inverting data represented by linear algebraic or integral equations," *Computer Physics Communications,* 27(3), 213-227.

[15] Provencher, S. W.(2014). "LCmodel & LCMgui User's Manual," *LCModel Version,* 6, 2-3.

[16] Cavassila, S., Deval, S., Huegen, C., Van Ormondt, D., and Graveron-Demilly, D.(2000), "Cramer-Rao bound expressions for parametric estimation of overlapping peaks: influence of prior knowledge," *Journal of Magnetic Resonance,* 143(2), 311-320.

[17] Cho, S. G., Kim, M. Y., Kim, H. J., Kim Y. S., Choi, W., Shin, S. H., Hong, K. C., Kim Y. B., Lee, J. H. and Suh, C. H.(2001), "Chronic hepatitis: in vivo proton MR spectroscopic evaluation of the liver and correlation with histopathologic findings," *Radiology,* 221(3), 740-746.

[18] Van Werven, J. R., Schreuder, T. C, M, A., Nederveen, A. J., Lavini. C., Jansen, P. L. M. and Stoker, J.(2010), "Hepatic unsaturated fatty acids in patients with non-alcoholic fatty liver disease assessed by 3.0T MR spectroscopy." *Journal of lipid research*, 75(2), e102-e107.

[19] Lee, Y. J., Jee, H. J., Noh, H. J., Kang, G. H., Park, J. Y., Cho, J. G., Cho, J. H., Ahn, S. D., Lee, C. H., Kim, O. H., Oh, B. C. and Kim, H. J.(2013), "In Vivo ^{1}H-MRS Hepatic Lipid Profiling in Nonalcoholic Fatty Liver Disease: An Animal Study at 9.4T," *Magnetic resonance in medicine,* 70(3), 620-629.

[20] Wang, D., Wei, Y. and Pagliassotti, M. J.(2006), "Saturated fatty acids promote endoplasmic reticulum stress and liver injury in rats with hepatic steatosis," *Endocrinology,* 147(2), 943-951.

[21] Cheung, J. S. Fan, S. J., Gao, D. S., Chow, A. M., Yang, J., Man, K. and Wu, E. X.(2011), "In vivo lipid profiling using proton magnetic resonance spectroscopy in an experimental liver fibrosis model," *Academic Radiology,* 18(3), 377-383